

Spin- and orbital-Hall effect in cyclic group symmetric metasurface

Yeon Ui Lee¹, Igor Ozerov², Frederic Bedu², Ji Su Kim¹, Frederic Fages², and Jeong Weon Wu^{1*}

¹Department of Physics, Quantum Metamaterial Research Center,

Ewha Womans University, Seoul 03760, Republic of Korea,

²Aix Marseille Univ, CNRS, CINaM, Marseille, France

(Dated: December 9, 2024)

ABSTRACT

Vortex beam carries orbital angular momentum (AM),[1] important in increasing the signal channels for communications.[2–4] Creation of vortex beams has been achieved by use of geometric phase in sub-wavelength diffraction grating[5] and liquid crystal q-plates[6]. Metasurface such as anisotropic planar structure is utilized to enhance spin-orbit interaction for spin-dependent shaping and control of the intensity and phase distributions.[7] High-efficiency spin-to-orbital AM conversion (SOC) has been demonstrated to generate vortex beams with high topological charges in the visible based on dielectric metasurfaces.[8] Here, we introduce a cyclic group symmetric metasurface (CGSM) to generate vortex beam exhibiting a spin- and orbital-AM dependent transverse shift in SOC. By designing CGSMs belonging to the cyclic group C_n , dynamical phase of cross-polarization scattered beam is altered according to the order n of cyclic group while keeping geometric phase constant. When n -fold rotational symmetry of azimuthal dynamical phase gradient is an odd integer n , there results a spin- and orbital-Hall effect.[9]

INTRODUCTION

Intrinsic optical Hall shift, spin-dependent or vortex charge-dependent, is an effect of fast degree of freedom (spin-AM or orbital-AM) on slow degree of freedom (beam trajectory), described by momentum-space Lorentz equation of motion in the presence of a Berry curvature of topological monopole. [10–12] Spin-dependent transverse shift of optical beam is also achieved by geometric Pancharatnam-Berry (PB) phase in a linear array of nano-antennas, called extrinsic optical spin Hall effect.[13, 14] The amount of shift is related to PB phase as shown in **Fig. 1 a, d, e**.[15]

In a circular array of nano-antennas with uniform width and length, even though not exhibiting spin-dependent transverse shift, spin-dependent PB phase is utilized to generate vortex beam by SOC in **Fig. 1 b, f, g**.[5, 6, 16–18] Polarization states in Poincaré sphere go through a circular trajectory twice providing the solid angle $\pm 8\pi$ corresponding to geometric phase $\pm 4\pi$, generating vortex beam of $l = \pm 2$, as shown in **Fig. 1 c**. Optical wave scattered from the circular array acquires

a phase factor, entirely geometric phase coming from a circular closed path \mathbf{C} in Stokes parameter space, leading to $\oint d\gamma(\mathbf{C}) = \pm 4\pi$ with a constant azimuthal PB phase gradient $\nabla_\phi \Phi_{PB} = \pm 2$. Therefore, the intensity profiles of $I_{-+}(r, \phi) = |E_{-+}|^2$ and $I_{+-}(r, \phi) = |E_{+-}|^2$ are degenerate even though helical phases are opposite for $l = \pm 2$, where $\{+-\}$ stands for left-circular polarization (LCP, σ_+) scattering / right-circular polarization (RCP, σ_-) incidence and $\{-+\}$ vice-versa. In fact, $E_{-+}(r, \phi) = J_2(k_0 r) e^{-k_0^2 r^2} \exp(i2\phi)$ and $E_{+-}(r, \phi) = J_{-2}(k_0 r) e^{-k_0^2 r^2} \exp(-i2\phi)$, where a constant $\nabla_\phi \Phi_{PB}$ leads to ϕ -independent amplitude $J_{\pm 2}(r) e^{-k_0^2 r^2}$ from the fact that each two neighboring nano-antennas provide an equal amount of PB phase during one full cycle, owing to rotational invariance of circular array of nano-antennas.

Without clarifying the underlying role of azimuthal phase gradient in giving rise to extrinsic spin- and orbital-Hall effect, degeneracy in OAM was lifted by rotational symmetry breaking to observe spin-dependent transverse shift of vortex beam in SOC.[9, 19–22] Consider a circular array of nano-antennas with different sizes from 1 to 16 in the range of $0 \leq \phi \leq 2\pi$, as shown in **Fig. 2 a**. Scattering wave from the circular array acquires a phase factor originating from both geometric phase $\gamma(\mathbf{C})$ and dynamical phase Φ_D ,[23] where $\gamma(\mathbf{C})$ is wavelength-independent while Φ_D has a frequency dispersion related to plasmonic resonances of each nano-antenna (see Supplementary Information). When rotational symmetry is broken, azimuthal dynamical phase gradient $\nabla_\phi \Phi_D(\phi)$ is ϕ -dependent, which results in ϕ -dependent amplitude of scattered wave, generating additional vortex beams with $l \neq 2$.[24, 25]

$$E(r, \phi)_{-+} = BG_2(r) f(r, \phi) \exp\{i2\phi + i\Phi_D^{+}(\phi)\} \\ = \sum_l^{\infty} \tilde{a}_l BG_l(r) e^{il\phi}$$

where scattering wave is partial-wave expanded in term of vortex beams of topological charge l with $BG_l(r) \equiv J_l(k_0 r) e^{-k_0^2 r^2}$, and expansion coefficients $\tilde{a}_l = a_l e^{i\psi_l}$ are complex, and $f(r, \phi) = 1$ when $\nabla_\phi \Phi_D^{+}$ vanishes. A similar expression holds for $E(r, \phi)_{+-}$.

Owing to the difference in scattering amplitudes from nano-antennas with different sizes, polarization states of scattered waves form a spiral trajectory on Poincaré sphere as shown in **Fig. 2 b**. In other words, solid angles subtended by polarization states between two neighboring nano-antennas are not constant. Rotational symmetry breaking introduced by nano-antennas with different sizes yields a spin-dependent non-constant azimuthal PB

* REVTeX Support: revtex@aps.org

phase gradient, $\nabla_\phi \Phi_{PB}$, permitting spin-dependent deflections in SOC as shown in **Fig. 2 c**.

Analysis of PB phase in rotation symmetry-broken circular array of nano-antennas shows that ϕ -dependence of beam profiles $I_{-+}(r, \phi)$ and $I_{+-}(r, \phi)$ is determined by the total phase $\Phi(\phi)^{-+} = 2\phi + \Phi_D^{-+}(\phi)$ and $\Phi(\phi)^{+-} = -2\phi + \Phi_D^{+-}(\phi)$ acquired by cross polarization scattering beam, where non-constant azimuthal dynamical phase gradients $\nabla_\phi \Phi_D$ are responsible for ϕ -dependence behavior of beam profiles. The occurrence of spin-dependent transverse shift, equivalent to non-vanishing $\Delta I \equiv I_{-+} - I_{+-}$, depends on the relation between $\Phi_D^{-+}(\phi)$ and $\Phi_D^{+-}(\phi)$ dictated by symmetry property of the circular array of nano-antennas with different sizes.

SAMPLE DESIGN AND MEASUREMENT

For a systematic study of relation between symmetry property of metasurface and spin-dependent transverse shift, tapered arc (TA) antennas are arranged in a circle to form metasurfaces belonging to cyclic group C_n , called tapered arc cyclic group symmetric metasurface (TA-CGSM), where in-plane inversion symmetry is determined by the order n of cyclic group, as shown in **Fig. 3 a**. Six different TA-CGSMs are fabricated, each TA-CSGM being composed of multiple TA antennas with varying width from 45nm to 150nm organized in 8 azimuthal segments of concentric rings repeated with 600nm radial spacing. **Fig. 3 b** shows optical microscope images of TA-CGSMs possessing C_∞ , C_1 , C_2 , C_3 , C_4 , C_5 , and C_6 symmetries, and SEM images of C_∞ and C_1 TA-CGSMs are shown in **Fig. 3 c**. Among experimental measurements in **Fig. 3 e, f**, C_∞ TA-CGSM exhibits degenerate ϕ -independent intensity profiles for I_{-+} and I_{+-} , while $C_n (n \neq \infty)$ TA-CGSMs exhibits ϕ -dependent intensity profiles of I_{-+} and I_{+-} , owing to non-constant azimuthal PB phase gradient Φ_{PB} coming from plasmonic resonance of TAs. Difference $\Delta I = I_{-+} - I_{+-}$ in **Fig. 3 g** corresponds to spin- and orbital-Hall shift, observed only in C_1 , C_3 , and C_5 TA-CGSMs (odd order n of C_n), where degeneracy of geometric structure is lifted by in-plane inversion symmetry breaking.[26] Vortex charge of cross-polarization scattering beam from $C_n (n \neq \infty)$ TA-CGSM is identified by an interference pattern between scattering vortex and incidence Gaussian beams, and counter-clockwise and clockwise twisted fringes confirm topological charges of $l = 2$ and $l = -2$ of I_{-+} and I_{+-} , respectively. See **Fig. S2** in Supplementary Information. FDTD calculation is in a perfect agreement with experimental results. See **Fig. S1** in Supplementary Information.

ANALYSIS

Vortex beam with topological charge l is described by Bessel-Gaussian beam $J_l(k_0 r) e^{-k_0^2 r^2} \exp(il\phi) = BG_l(r) \exp(il\phi)$.[27] In order to clarify how the addition

of dynamical phase to geometric phase in SOC alters ϕ -dependence of phases $\Phi^{-+}(\phi)$ and $\Phi^{+-}(\phi)$, experimentally measured intensity profiles in **Fig. 3 e, f** are fit as a linear superposition of vortex beams, as shown in **Fig. 4 a, b** along with phases in **Fig. 4 d, e**. The fit values of partial-wave expansion coefficients \tilde{a}_l are listed in **Table 1** of Supplementary Information. We observe two important features. First, phases of $E_{-+}(\phi)$ and $E_{+-}(\phi)$ are opposite, i.e., $\Phi^{-+}(\phi) = -\Phi^{+-}(\phi)$, which is from the opposite senses of rotation of polarization state trajectories on Poincaré sphere for $\{-+\}$ and $\{+-\}$. Second, intensity profile $I_{+-}(\phi)$ is the same as that of in-plane inversion symmetry operated $I_{-+}(\phi)$, i.e., $I_{+-}(\phi) = I_{-+}(\phi + \pi)$, as a result of $\Phi^{-+}(\phi) = -\Phi^{+-}(\phi)$. The two features immediately explain why spin- and orbital-Hall effect takes place only for C_n with odd n . For even n , ΔI vanishes identically, since geometric structures possess in-plane inversion symmetry.

Contributions of dynamical phase are further clarified. First, we expect a correlation between intensity profile and ϕ -dependence of phase. As shown in **Fig. 5** for C_1 TA-CGSM, $E_{-+}(\phi)$ and $E_{+-}(\phi)$ have a local maximum at the azimuthal angles ϕ where the absolute value $|\nabla_\phi \Phi_D|$ is a local minimum. Helical wavefronts with azimuthal geometric phase gradient ± 2 are altered by introduction of non-constant azimuthal dynamical phase gradient $\nabla_\phi \Phi_D$, to build focused spots along azimuthal direction, similar to wavefront modification when a plane wave goes through a medium with spatially varying index.[28] Refer to Supplementary Information for C_n TA-CGSMs with n other than 1. The intensity profile possesses a feature of OAM superposition states, useful for quantum information systems.[29]

Second, the phase ψ_l of partial-wave expansion coefficient \tilde{a}_l is related to dynamical phase $\Phi_D(\phi)$ (Supplementary Information), determining interference behavior between partial-wave vortex beams having difference topological charge ls . C_4 and C_5 TA-CGSMs are closely examined in the left panel (**Fig. 4 f, g, h, i**) and right panel (**Fig. 4 j, k, l, m**). In C_4 TA-CGSM $E_{-+} = BG_2 \exp\{i2\phi\} + 0.24BG_{-2} \exp\{-i2\phi\} \exp\{+i\frac{3\pi}{2}\}$ and $E_{+-} = BG_{-2} \exp\{-i2\phi\} + 0.24BG_2 \exp\{i2\phi\} \exp\{-i\frac{3\pi}{2}\}$, where azimuthal angles for constructive and destructive interferences are the same for E_{-+} and E_{+-} , resulting in $\Delta I = 0$. In C_5 TA-CGSM $E_{-+} = BG_2 \exp\{i2\phi\} + BG_{-3} \exp\{-i3\phi\} \exp\{+i\pi\}$ and $E_{+-} = BG_{-2} \exp\{-i2\phi\} + BG_3 \exp\{i3\phi\} \exp\{-i\pi\}$, where azimuthal angles for constructive and destructive interferences differ by 0.2π for E_{-+} and E_{+-} , and $\Delta I \neq 0$ leading to non-vanishing spin-dependent transverse shift. Third, a frequency dispersion of dynamical phase due to the plasmonic resonance of TA renders intensity profiles to be dependent on incidence beam wavelength, confirmed to be true as shown in Supplementary Information.

CONCLUSIONS

In summary we demonstrated spin- and orbital-Hall effect in metasurfaces possessing cyclic point group symmetry C_n . Lifting degeneracy in orbital angular momentum is achieved by selectively controlling the symmetry order n . By identifying the role of dynamical phase in giving rise to spin-dependent transverse shift in SOC, spatial separation and modification of vortex beam profile are made possible. This new approach provides significant advantages in applications such as vortex multiplexing in communication device and vortex beam analyzer as well as fundamental understanding of interactions among angular momenta of light in metasurface.

METHODS

Fabrication of cyclic symmetric metasurfaces

We used 1mm thick borosilicate glass round substrates with diameter of one inch (UQG Optics). First, the substrates were cleaned in sequential bathes of acetone and isopropanol, assisted by ultrasonication. Then the substrates were rinsed in deionized water and dried by nitrogen flow followed by oxygen radical plasma treatment in a barrel reactor (Nanoplas, France) to activate the glass surface. Second, an electron beam resist (PMMA, ARP 679) and a conductive polymer (SX AR PC 5000/90.2 from Allresist, Germany) layers were successively spin-coated. The thickness of the resulting layer was chosen to be about 70 nm and it was measured by a contact profilometer (DektakXT, Bruker, Germany) after e-beam exposition and resist development. Third, we used an e-beam lithography (EBL) tool (Pioneer, Raith, Germany) for sample patterning. We used 20 kV acceleration voltage of the electron gun, and the beam current was 0.016

nA for the aperture of $7.5 \mu\text{m}$. The typical working distance was about 5 mm, and the nominal exposition dose was chosen in the range from 100 to $180 \mu\text{C}/\text{cm}^2$. Forth, two successive metal layers (Cr, 3nm for seeding and Au, 27 nm) were deposited by thermal evaporation (Auto 306, Edwards, UK). The thickness was monitored by quartz crystal microbalance during the deposition and measured by a contact profilometer after lift-off process. The lift-off was done in ethyl lactate solution, followed by rinsing and nitrogen drying. Finally, the samples were observed by optical and scanning electron microscopy (SEM). For SEM observation, we used low acceleration voltage of 3kV in order to decrease the sample charging because the glass substrate is insulating. (For more information, see Supplementary Information)

Calculation of Stokes parameters

To analyze vortex beam generation, we investigate Stokes parameters of space-variant nano-antennas as optical elements of TA-CGSMs on Poincaré sphere. On Poincaré sphere, any point in the equator, the north and south poles correspond to the linear polarization, right-circular and left-circular polarization state, respectively. We calculated Stokes parameters of scattered light at wavelength of 1310nm from each nano-antennas with finite difference time domain (FDTD) method. We defined the Stokes parameters as follows. S_0 is the total intensity, S_1 is the intensity of the horizontal linear component minus the intensity of the vertical linear component, S_2 is the intensity of the diagonal linear component minus the intensity of the antidiagonal linear component, and S_3 is the intensity of the right circular component minus the intensity of the left circular component. The normalized Stokes parameter $s_1 = S_1/S_0$, $s_2 = S_2/S_0$, and $s_3 = S_3/S_0$ are plotted on the surface of Poincaré sphere.

-
- [1] Allen, L., Beijersbergen, M. W., Spreeuw, R. & Woerdman, J. Orbital angular momentum of light and the transformation of laguerre-gaussian laser modes. *Physical Review A* **45**, 8185 (1992).
- [2] Bozinovic, N. *et al.* Terabit-scale orbital angular momentum mode division multiplexing in fibers. *Science* **340**, 1545–1548 (2013).
- [3] Ren, H., Li, X., Zhang, Q. & Gu, M. On-chip noninterference angular momentum multiplexing of broadband light. *Science* **352**, 805–809 (2016).
- [4] Yang, K. *et al.* Wavelength-selective orbital angular momentum generation based on a plasmonic metasurface. *Nanoscale* (2016).
- [5] Biener, G., Niv, A., Kleiner, V. & Hasman, E. Formation of helical beams by use of panchromatic–berry phase optical elements. *Optics letters* **27**, 1875–1877 (2002).
- [6] Marrucci, L., Manzo, C. & Paparo, D. Optical spin-to-orbital angular momentum conversion in inhomogeneous anisotropic media. *Physical review letters* **96**, 163905 (2006).
- [7] Bliokh, K., Rodríguez-Fortuño, F., Nori, F. & Zayats, A. V. Spin-orbit interactions of light. *Nature Photonics* **9**, 796–808 (2015).
- [8] Devlin, R. C. *et al.* Spin-to-orbital angular momentum conversion in dielectric metasurfaces. *arXiv preprint arXiv:1605.03899* (2016).
- [9] Bliokh, K. Y., Alonso, M. A., Ostrovskaya, E. A. & Aiello, A. Angular momenta and spin-orbit interaction of nonparaxial light in free space. *Physical Review A* **82**, 063825 (2010).
- [10] Berry, M. The quantum phase, five years after. In Andrews, D. L. & Babiker, M. (eds.) *Geometric phases in physics* (World Scientific Singapore, 1989).
- [11] Onoda, M., Murakami, S. & Nagaosa, N. Hall effect of light. *Physical review letters* **93**, 083901 (2004).
- [12] Bliokh, K. Y., Niv, A., Kleiner, V. & Hasman, E. Geometrodynamics of spinning light. *Nature Photonics* **2**, 748–753 (2008).
- [13] Shitrit, N. *et al.* Spin-optical metamaterial route to spin-controlled photonics. *Science* **340**, 724–726 (2013).

- [14] Cardano, F. & Marrucci, L. Spin-orbit photonics. *Nature Photonics* **9**, 776–778 (2015).
- [15] Luo, W., Xiao, S., He, Q., Sun, S. & Zhou, L. Photonic spin hall effect with nearly 100% efficiency. *Advanced Optical Materials* **3**, 1102–1108 (2015).
- [16] Brasselet, E., Gervinskas, G., Seniutinas, G. & Juodkazis, S. Topological shaping of light by closed-path nanoslits. *Physical review letters* **111**, 193901 (2013).
- [17] Karimi, E. *et al.* Generating optical orbital angular momentum at visible wavelengths using a plasmonic metasurface. *Light Sci. Appl* **3**, e167 (2014).
- [18] Osorio, C. I., Mohtashami, A. & Koenderink, A. F. K-space polarimetry of bullseye plasmon antennas. *Scientific reports* **5** (2015).
- [19] Shitrit, N., Bretner, I., Gorodetski, Y., Kleiner, V. & Hasman, E. Optical spin hall effects in plasmonic chains. *Nano letters* **11**, 2038–2042 (2011).
- [20] Shitrit, N., Maayani, S., Veksler, D., Kleiner, V. & Hasman, E. Rashba-type plasmonic metasurface. *Optics letters* **38**, 4358–4361 (2013).
- [21] Liu, Y. *et al.* Photonic spin hall effect in dielectric metasurfaces with rotational symmetry breaking. *Optics letters* **40**, 756–759 (2015).
- [22] Ling, X. *et al.* Giant photonic spin hall effect in momentum space in a structured metamaterial with spatially varying birefringence. *Light: Science & Applications* **4**, e290 (2015).
- [23] Berry, M. V. Quantal phase factors accompanying adiabatic changes. *Proceedings of the Royal Society of London A: Mathematical, Physical and Engineering Sciences* **392**, 45–57 (1984).
- [24] Kotlyar, V., Kovalev, A. & Soifer, V. Asymmetric bessel modes. *Optics Letters* **39**, 2395–2398 (2014).
- [25] Kotlyar, V., Kovalev, A., Skidanov, R. & Soifer, V. Asymmetric bessel–gauss beams. *JOSA A* **31**, 1977–1983 (2014).
- [26] Slobozhanyuk, A. P. *et al.* Enhanced photonic spin hall effect with subwavelength topological edge states. *Laser & Photonics Reviews* (2016).
- [27] Mendoza-Hernández, J., Arroyo-Carrasco, M. L., Iturbe-Castillo, M. D. & Chávez-Cerda, S. Laguerre–gauss beams versus bessel beams showdown: peer comparison. *Optics letters* **40**, 3739–3742 (2015).
- [28] Saleh, B. E., Teich, M. C. & Saleh, B. E. *Fundamentals of photonics*, vol. 22 (Wiley New York, 1991).
- [29] Franke-Arnold, S. & Jeffers, J. Orbital angular momentum in quantum communication and information. *Structured Light and Its Applications*, ed. Andrews, DL 271–29 (2008).

ACKNOWLEDGEMENT

JWW acknowledges the support from the Ministry of Science, ICT & Future Planning, Korea (2015001948, 2014M3A6B3063706). Nanofabrication processes were performed in PLANETE cleanroom facility, CT PACA.

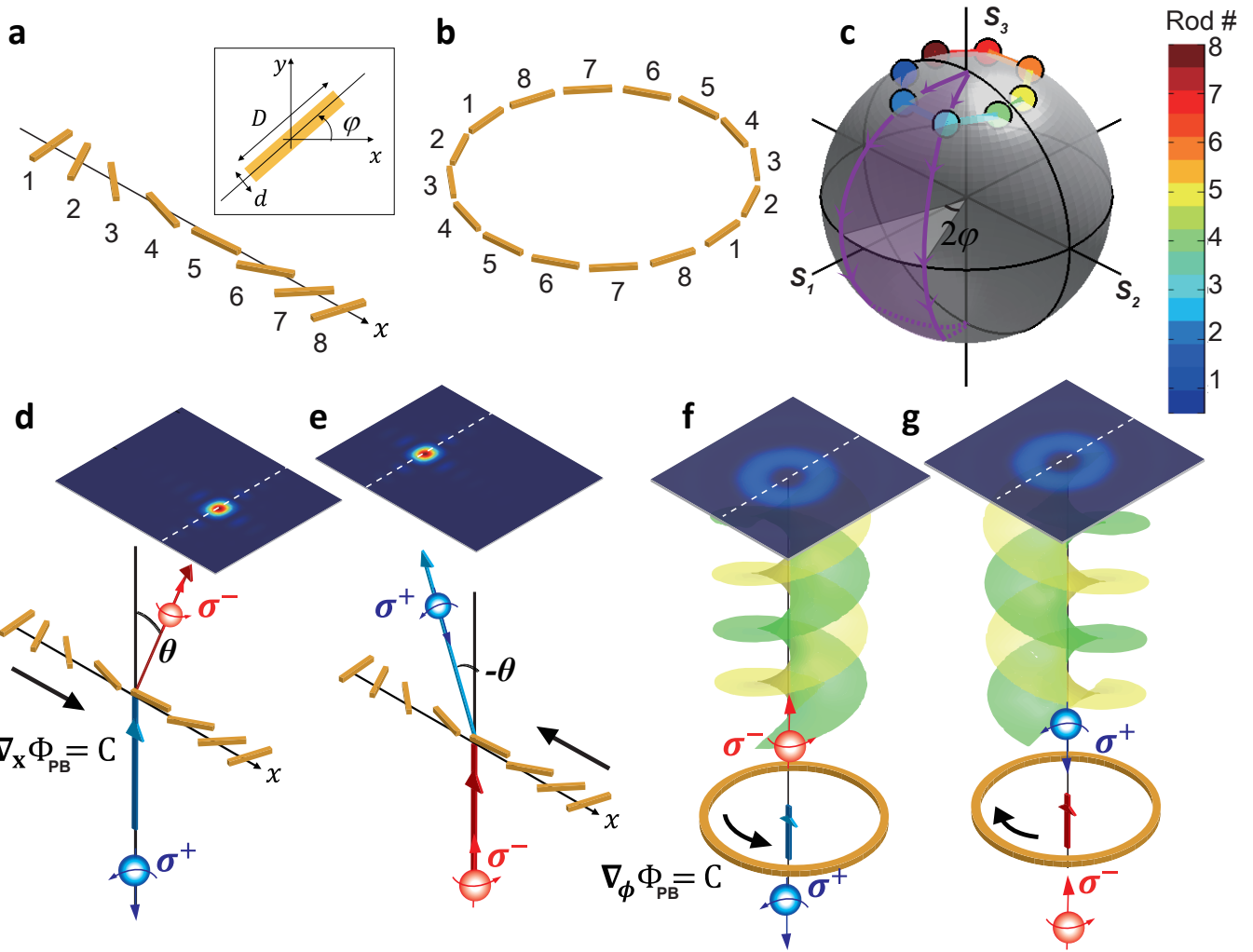


FIG. 1. Array of nano-antennas with a constant PB phase-gradient and Poincaré sphere plot of Stokes parameters. Inset figure shows a schematic of rotated nano-antenna with length D and width d making an angle φ with x -axis. **a**, Linear array of rotating nano-antennas from 1 to 8 **b**, circular array of nano-antennas from 1 to 8 in the range of $0 \leq \phi \leq \pi$ and from 1 to 8 in the range of $\pi \leq \phi \leq 2\pi$ **c**, Poincaré sphere plot of Stokes parameters of optical beams scattered from nano-antennas of (a) and (b) for LCP incident beam. Color code corresponds to the nano-antenna number. **d,e**, spin-dependent deflection of cross-polarization scattered optical beam shown up as extrinsic spin Hall effect. $+x$ -direction deflection of RCP (σ_-) beam for LCP (σ_+) incidence beam in (d) and the opposite deflection in (e). **f,g**, generation of $l = +2$ vortex scattered beam of RCP (σ_-) for Gaussian incidence beam of LCP (σ_+) in (f) and the vortex with sign of topological charge reversed in (g).

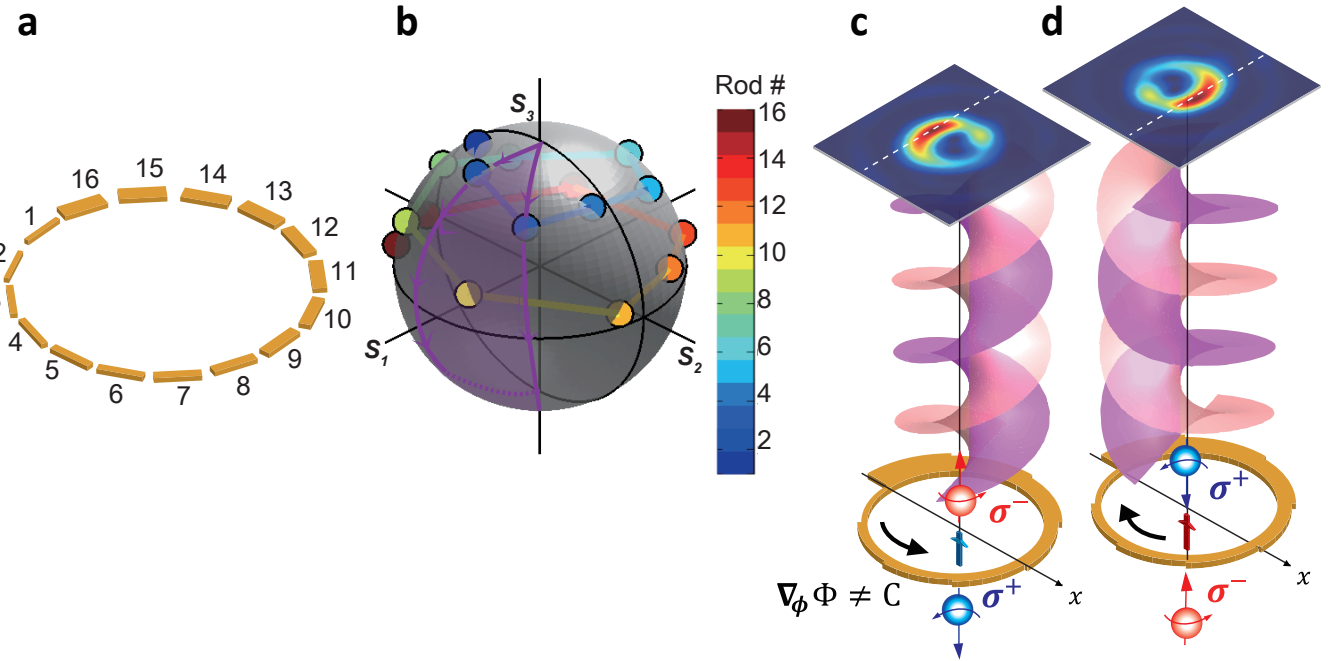


FIG. 2. **Array of nano-antennas with a non-constant PB phase-gradient and Poincaré sphere plot of Stokes parameters.** **a**, circular array of nano-antennas with varying width from 1 to 16 in the range of $0 \leq \phi \leq 2\pi$ **b**, Poincaré sphere plot of Stokes parameters of optical beams scattered from nano-antennas of (a) and (b) for LCP incidence beam. Color code corresponds to the nano-antenna number. **c,d**, spin and orbital angular momentum dependent beam profiles shown up as spin- and orbital-Hall effect. Scattered beam of RCP (σ_-) has the beam center of gravity shifted along $-x$ -direction with asymmetric vortex beam profile for Gaussian incidence beam of LCP (σ_+) and the opposite shift and the vortex with sign of topological charge reversed in (d).

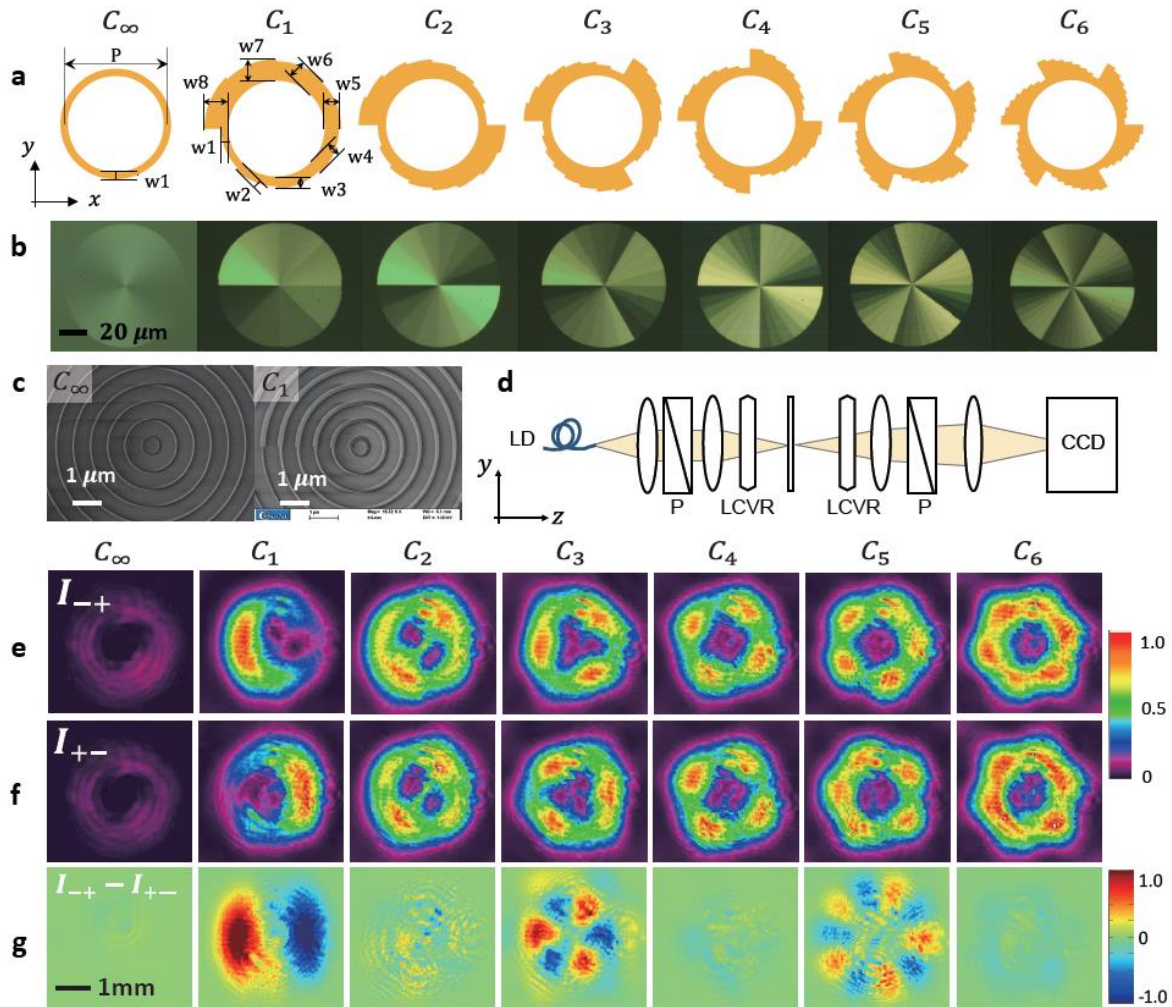


FIG. 3. **Cyclic group symmetric metasurfaces and extrinsic spin- and orbital-Hall effect.** **a**, Designed TA-CGSM with C_{∞} , C_1 , C_2 , C_3 , C_4 , C_5 , and C_6 symmetry, respectively. The periodicity is denoted by $p = 600\text{nm}$, and widths of arcs are by $w_1 = 45\text{nm}$, $w_2 = 60\text{nm}$, $w_3 = 75\text{nm}$, $w_4 = 90\text{nm}$, $w_5 = 105\text{nm}$, $w_6 = 120\text{nm}$, $w_7 = 135\text{nm}$, and $w_8 = 150\text{nm}$. **b**, Optical microscope images of fabricated TA-CGSMs belonging to C_{∞} , C_1 , C_2 , C_3 , C_4 , C_5 , and C_6 symmetry, respectively. **c**, SEM images of fabricated TA-CGSMs belonging to C_{∞} and C_1 with scale bars of $1\mu\text{m}$. **d**, Experimental setup for spin- and orbital-Hall effect measurement. **e**, **f**, Far-field intensity distributions scattered from TA-CGSM of C_{∞} , C_1 , C_2 , C_3 , C_4 , C_5 , and C_6 for I_{-+} and I_{+-} , respectively, measured with $\lambda = 1310\text{nm}$ incidence beam. **g**, Plot of the difference $I_{-+} - I_{+-}$ corresponding to extrinsic spin- and orbital-Hall effect.

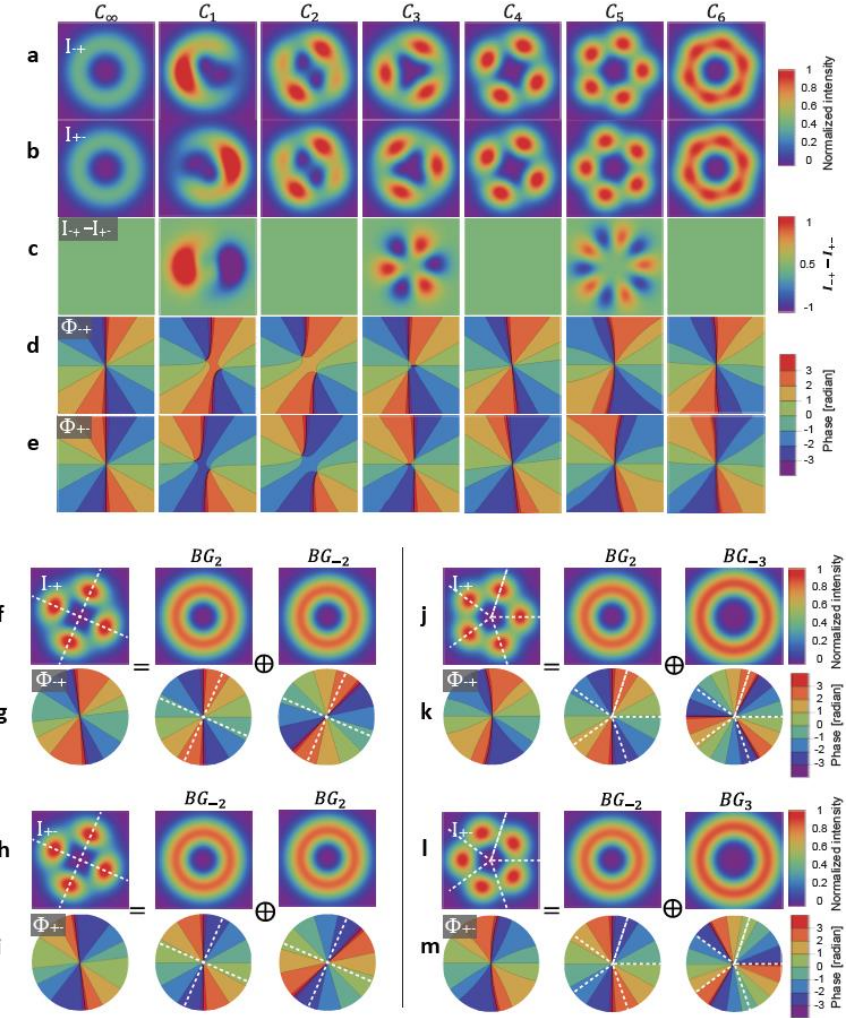


FIG. 4. **Analytically calculated extrinsic spin and orbital Hall effect for cyclic group symmetric metasurfaces.** Calculated far-field intensity (a, b). c, Calculated $I_{+-} - I_{-+}$, and phase distributions (d, e) of spin flip component for $C_\infty, C_1, C_2, C_3, C_4, C_5$, and C_6 CGSM. f-i (j-m), Fourier decomposition of E_{-+} and E_{+-} of C_4 (C_5) CGSM.

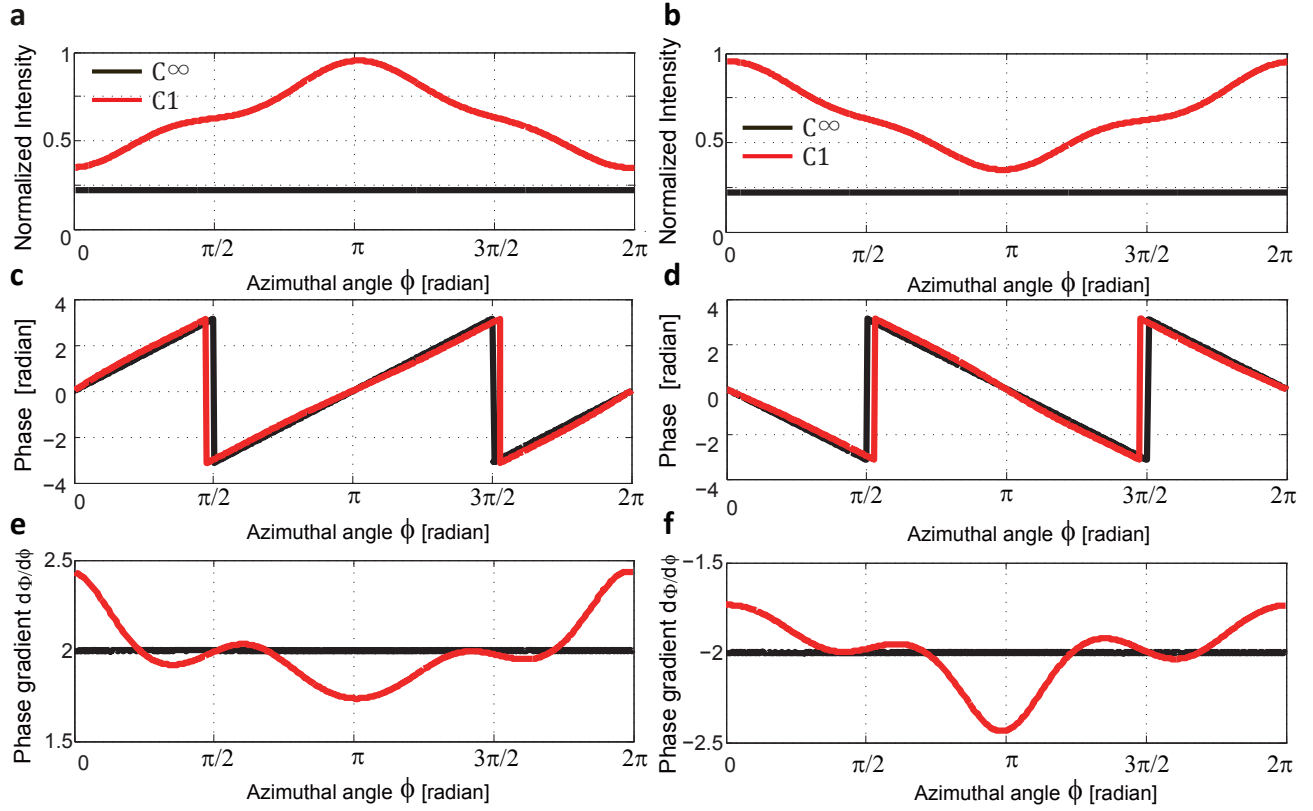


FIG. 5. **Analytically calculated intensity, phase, and phase gradient as a function of the azimuthal angle.** **a,b**, Intensity, **c,d**, phase, **e,f**, uniform phase gradient of C_∞ (black) and nonuniform phase gradient of C_1 (red) for $\{ij\}$ configuration, where $\{ij\}$ are detection and incidence circular polarization helicity, left- $(+)$ and right- $(-)$ circular polarization. The nonuniform phase gradient can be considered by introducing the anisotropy.